Published in final edited form as:
Int J Radiat Oncol Biol Phys. 2005 September 1; 63(1): 290–300. doi:10.1016/j.ijrobp.2005.05.025.

An analysis of an implantable dosimeter system for external beam therapy

Robert D. Black, Ph.D.[a,*], **Charles W. Scarantino, M.D., Ph.D.**[a,c], **Gregory G. Mann, M.S.**[a], **Mitchell S. Anscher, M.D.**[b], **Robert D. Ornitz, M.D.**[c], and **Benjamin E. Nelms, Ph.D.**[d]
a *Sicel Technologies, Morrisville, NC, USA 27560*

b *Duke U. Medical Center, Durham, NC, USA 27710*

c *Rex Healthcare, Raleigh, NC, USA 27607*

d *CMS, Inc., St. Louis, MO, USA 63132*

Abstract

Background and purpose—To review the data from an implantable radiation dosimetry system used in a clinical setting and examine correlations between dosimeter readings and potential causative error sources.

Material and methods—MOSFET-based, encapsulated dosimeters were evaluated in a phantom (*in vitro*) and in a study with 18 patients. The dosimeters were placed in the gross tumor volume or in collateral normal tissue. Predicted dose values were established by imaging the dosimeters in the planning CT's.

Results—The *in vitro* study confirmed that bounding cumulative errors due to setup, planning, and machine output within a +/−5% level is achievable. In patients, it was found that deviations from the targeted dose often exceeded the 5% level.

Conclusions—The use of an implantable dosimeter system could provide an effective empirical check on the dose delivered at depth. Such a tool may have value for institutional QA as well as for therapy delivered to individual patients.

Keywords

implantable dosimeter; radiation therapy; *in vivo* dosimetry

Introduction

The need to ensure accurate delivery of dose at depth during external beam therapy treatments is well accepted (1). A conformal treatment modality like IMRT (intensity-modulated radiation therapy) has resulted in increased attention to *in vitro* plan verification (2,3) though the need for individualized checks on every patient plan has been debated (4). Compensatory targeting aids, such as ultrasound localization and x-ray based IGRT (image-guided radiation therapy), have emerged to address the need for better targeting assurance. The performance of some of these new localization tools has been examined (5,6,7,8,9). The obvious appeal of the goal of providing an escalated dose to tumor while sparing more normal tissue has led to clinical acceptance prior to the arrival of compelling long-term outcome data (10). Recently, a debate

*Corresponding author: Robert Black, Ph.D., Sicel Technologies, 3800 Gateway Center Blvd., Suite 308, Morrisville, NC, 27560, USA, phone: 919-465-2236, fax: 919-465-0153, e-mail: bblack@siceltech.com.

has even been aired (11) addressing the legitimacy of NRC radiation therapy medical event guidelines. What constitutes an acceptable dose error and what empirical data exist to shed light on the issue?

The history of external beam therapy has been highly empirical. Dose protocols have been established in an iterative fashion, bracketing the clinical dose realm with inadequate response and unacceptable normal tissue sequela (12,13). Indeed, the likely variations in individual responses to radiation at a given dose level are largely unknowable prior to treatment. For example, well-established results are reported *in vitro* with regard to the importance of the partial pressure of oxygen in a tumor and yet this knowledge has not been easy to utilize clinically (14). It is both difficult to measure pO_2 levels and influence them even if they are established. However, a far more basic lack of information has hindered a true quantitative analysis of dose control and that is an accurate, measured value of dose delivered at depth. Without an independent bench mark of the true dose delivered to a region the twin influences of individual variation in response and inadequate dose control cannot be separated. Stated differently, what percentage of therapy failures result from failed dose delivery?

Standards such as TG-51 (15) guide quality assurance (QA) for linear accelerators. Clearly the accuracy of radiation therapy procedures relies on robust therapy machine calibration. QA for this function is well developed and significant intrinsic linac errors are expected to be rare in general practice. However, the advent of complex field pattern formation using multileaf collimators has heightened the need for additional scrutiny and testing that continues after commissioning (2,3). Mechanical systems checks now demand increasing time from physics staff and the adoption of the inverse planning approach with IMRT challenges the intuition of users.

Complementing the reference dosimetry protocol, TG-51, is TG-53 (16), which outlines key quality assurance tasks for radiation therapy treatment planning more broadly. Quoting from this source, it seeks to "…guide and assist the clinical medical physicist in developing and implementing a comprehensive but viable program of quality assurance for modern radiotherapy treatment planning…encompassing image-based definition of patient anatomy, 3D beam descriptions for complex beams including multileaf collimator apertures, 3D dose calculation algorithms, and complex plan evaluation tools including dose volume histograms. The Task Group recommends a…program which is individualized to the needs of each institution…." The need to address QA in a way that is matched to a specific institution is a seminal point since not all centers have the same resources. Tools that can enhance cross-institutional dose consistency are important in this regard.

What is often discounted is that the process of simulating and creating a therapy plan for a specific patient is a theoretical projection and that process does not have the same empirical standing as the machine-based measurements. As noted above, the complexity of IMRT plans has created such concern that they are applied to a phantom for confirmation before delivery to the patient (2,3,17). The algorithms used in modern therapy planning software are becoming progressively more sophisticated but, on the other hand, it is still common to find clinics wherein inhomogeneity correction is not applied to lung plans despite clear evidence that this leads to a change in delivered dose (18,19,20). The use of surface dosimeters on patients can provide a useful addition to basic machine QA (21). Interpolating a mid-plane dose from entrance and exit dose measurements can be a useful check. However, these devices cannot be used to verify actual dose values at depth (consider, for example, the utility of a surface dosimeter in the case where the target has shifted its position internally).

An additional assumption that is frequently made is that a static CT dataset taken prior to the commencement of therapy will be representative of that patient several weeks into therapy.

The accommodation of anticipated change is reflected in the sequentially expanding margins from the GTV to the PTV, but the breadth of these margins is being reduced in modalities like IMRT. This clash of assumptions has given birth to the various daily localization schemes that attempt to maintain a consistent isocenter and avoid marginal misses that could compromise therapy. Recently the obvious question of how such re-centering impacts the validity of the original radiation therapy plan has been addressed in clinical studies (e.g., 5).

Patient setup errors, intrafractional and interfractional movement of the tumor, and radiation therapy plan errors create a web of dependent and independent error sources that can be prohibitively difficult to track in the clinic (22). Ultimately, it is the net effect of these influences on delivered dose that matters (23). The use of dosimeters that are implanted into representative target regions provides the first empirical means of verifying dose at depth. The study described below evaluates clinical experience with such a device and demonstrates with illustrative cases how this dose data can be used to identify or at least narrow the list of possible error sources leading to an incorrect dose. It is emphasized that this device is fully consistent with existing and evolving tools aimed at ensuring proper dose control. It is crucial to emphasize that the import of all dose discrepancies to clinical outcomes cannot at present be clearly established. It will be through a reanalysis of dose-response across a wide range of subjects that the variability in response due to dosing error can be removed from the host of true physiologic factors affecting outcome.

Methods and Materials

Sensor system

The device employed in this study is an implantable radiation dosimeter capsule that uses a MOSFET (metal-oxide-semiconductor field effect transistor) as the radiation-sensing element (24,25,26). It is important to note that this MOSFET is specifically made to be sensitive to radiation exposure in the therapeutic dose range whereas the supporting microelectronic devices in the sensor body are radiation-hard in this range. The active area of the MOSFET is 690x15 μm and thus may be viewed as a point detector. The MOSFET accumulates positive charge at the semiconductor/oxide interface. This charge is created by collisional processes involving the secondary electrons associated with the therapy beam. Though the sensitive region of the MOSFET is small, the size scale of what it senses is dictated by the dose gradient in which it sits. The mean-free-path of the secondary electrons, which ultimately limits the sharpness of dose gradients, will always be large compared to the active area of the MOSFET. In other words, the MOSFET will not record deposited energy density to a resolution of 690 x 15 μm because the dose pattern itself will never be that fine-grained. The capsule is hermetically sealed so that it is able to remain permanently in the body. Communication to the device is achieved telemetrically and this allows for daily readings of the device during each therapy session. The location of the MOSFET is established by visualization of the sensor in the planning CT. Because the device is actually disposed in the target tissue, comparison of true delivered dose relative to predictions given by the isodose plan are enabled. Additionally, the device can be seen with diagnostic-energy x-rays and ultrasound (e.g., transrectal ultrasound was used to guide placement in the prostate patients). Thus it serves a secondary role as a fiducial marker.

In vitro test study

So as to examine the efficacy of the implanted dosimeter in a simulated clinical setting, an acrylic phantom (Quasar, Modus Medical) was adapted to hold a reference ion chamber and two water-heated dosimeters simultaneously (27). Heated water (37°C) was circulated through hoses into holders in which the sensors were fixed. It is important to keep the sensors at a fixed temperature during the reading process to avoid thermal drift in the readings (24). (Of course

this is a requirement easily met *in vivo*.) The sensors are maintained at body temperature in between irradiation sessions so as to match the conditions under which they were calibrated.

The phantom allowed for a variety of interesting configurations and three different arrangements were evaluated: 1) all three dosimeters arranged linearly on the left edge of a 4-beam field set, 2) one of the dosimeters offset laterally in the penumbra region of the AP/PA field set, and 3) configuration #1 with a lung-equivalent material substituted for an acrylic block in the lateral beam path. Figure 1 shows a schematic of the sensors and phantom. Sensor 1 can orbit the ion chamber without changing the positions of the other devices.

Each of the three configurations was separately planned using a common treatment planning system (Pinnacle 6.2b, Philips Medical Systems). A Clinac 2100 (Varian Medical Systems) was used for all runs with a nominal beam energy of 18 MV. The planning grid was 0.4 cm in each dimension. Heterogeneity correction was used and the TPS uses an adaptive convolution algorithm. Room lasers were used to align the phantom, which has well-defined markings, each day. SSD was measured with respect to the nearest face for each of the 4 fields. The sensitive areas of the implanted dosimeters are easily identified by CT and predicted values were established by performing a point-dose query in the isodose contour space by locating the image voxel containing the MOSFET (no volume averaging around the MOSFET location was performed). Since pre- and post-fraction measurements are taken for each exposure, additional dose contributed by CT imaging is not a factor. The ion chamber serves to validate the machine output during a given session. Ion chamber readings were corrected for temperature and pressure on a daily basis. The dosimeters are pre-calibrated at body temperature in a protocol that delivers five consecutive daily doses of about 200 cGy to all devices (24). Reference devices are then given additional 200 cGy per day fractions out to 70–80 Gy. A third-order polynomial fit is applied to the reference devices to generate a calibration curve for the experimental devices, which is accurate at least over the daily dose range from 180–220 cGy. The phantom has well-defined target areas for alignment and is mechanically solid so that excellent alignment reproducibility is possible. The homogeneity of the phantom material leads to a very tractable planning problem for commercial TPS algorithms. Thus the phantom presents an idealized test bed for evaluating sensor performance in the absence of target motion and planning challenges.

Clinical sensor placement

The first ten patients recruited for sensor placement had unresectable disease (25) and the next eight were recruited from a population that included resectable disease as well. Two institutions (Rex Healthcare, Raleigh, NC and Duke University School of Medicine, Durham, NC) were involved in patient recruitment. The FDA (U.S. Food & Drug Administration) and the Institutional Review Boards of Rex Healthcare and Duke University approved the study.

Following device implantation, all patients underwent computed tomography (CT) simulation in the treatment position. Table 1 includes details about specific patient treatment parameters. All planned doses at sensor locations were in the range of 180–220 cGy per fraction with the exception of some sensors during electron boosts (breast patients) and one short boost period to a rectal patient (04). The implant was identified on the planning CT and predicted dose values were associated with the relevant sensor position. Patients were required to receive at least 4 weeks of treatment and daily fractions. The sensor was interrogated prior to and following each fraction of radiation to obtain the dose delivered to the sensor position. The results were recorded and compared to the expected dose of radiation.

Methods for analyzing clinical sensor data

Bar graphs of the daily dose values versus predicted values provided a visually effective means of showing qualitative trends (e.g., under- or overdosing). It was also helpful to establish a common scale on the dose axis to allow for more direct comparisons between patients undergoing similar treatments. Computing the standard deviation of dose readings (relative to the sensor dose mean) over a given field configuration allows for a distinction between random and systematic dose errors based on the magnitude of the standard deviation value relative to the sensor tolerance. That is, if the absolute error due to the sensor itself accounts for the daily deviations seen in the patient, then one can conclude that the dose contours in the area of the sensor don't vary significantly. However, if the standard deviation of the readings exceeds the sensor tolerance significantly there must be a random variation in the sensor position in the dose contours. It was also instructive to plot histograms of dose deviations (planned versus measured) for patients undergoing the same treatment (a standard protocol for a disease site at a given institution). This method allowed for a clear assessment of procedural norms and the data showed a generally Gaussian character, illuminating the mean and standard deviation for each tumor site.

Results

Phantom Testing

Figure 2 shows the results of the *in vitro* study using the phantom. The standard deviation values for both implanted sensors were within expected device tolerance (1.8% for sensor 1 and 1.9% for sensor 2). The standard deviation for the ion chamber readings was 1.4% and at least some of this is attributable to random alignment error and beam output variation. Sensor 2 was in a region of relatively high gradients and so the low standard deviation value measured suggests that there was no systematic problem in obtaining adequate alignment accuracy. The sensor 1&2 predicted values were adjusted by the ion chamber readings. This adjustment should address beam output variations, but does not directly address alignment errors.

Radiation therapy plans with and without inhomogeneity correction were generated (the corrected values were used in the quoted results). The 3 different configurations of the sensors are labeled as "TPS 1–3" in figure 2. It should be noted that the x-ray density of the acrylic phantom is higher than that of water. The TPS was self-consistent in that it used correction factors based on electron density values derived from the planning CT's. The plans without correction overestimated dose by 3.0–3.5%. Interestingly, there was no significant difference seen in the general agreement between the measured and predicted results as a function of the three configurations. A phantom system of this sort is very useful in assessing the magnitude of errors due to setup alignment (for a rigid target, of course), machine output, treatment plan error (for a simple, homogeneous target), and intrinsic sensor error. Not surprisingly, an idealized test of this sort reflects the fact that responsible institutional QA programs are effective in creating excellent reproducibility in dose delivery. However, it must be noted that during one planned session (day 5) the ion chamber value read over 5% high, indicating an overdose was delivered by the machine and thus the data point was dropped.

During the time that sensor 1 was rotated, it received a dose of roughly 104 cGy versus a dose of 183 cGy in the un-rotated position. The device calibration curve used for the sensors assumes that they will see nominal doses in the 180–220 cGy range. Underdosing of the magnitude seen by the rotated sensor 1 leads to a small overshoot (2–3%) in the measured dose value and this was taken into account in figure 2. The origin of this effect relates to a property of MOSFET's exposed to radiation (termed fade) that leads to a daily dose-dependent sensitivity in long-term calibration of the MOSFET. This effect was not relevant to the patient dose fractions delivered in this study except possibly during an electron boost with some breast patients as noted above,

but measurements in very low dose regions or measurements in an accelerated dose protocol would need to take the effect into account. It is certainly possible to accommodate this effect by creating a series of corrections for larger or smaller dose fractions. For the purpose of this study, the 180–220 cGy range was adequate.

In clinical practice, ion chambers tend to be reserved for machine calibration and surface dosimeters are utilized (in an analogous way) to estimate entry or exit doses for actual patients. In particular, the use of buildup with a surface dosimeter will provide a d_{max} measurement that can be compared with TPS predictions. Facilities that use surface dosimetry generally restrict usage to initial confirmation of field values and when fields are changed. Occasionally, dosimetry will be repeated for the same field if target alignment questions arise. The implantable sensor described herein can be read in under 5 seconds and thus dose data can be collected easily on a daily basis. The implantable sensor also creates the potential to model IMRT delivery in a phantom containing sensors and then follow conformance to the plan *in vivo* with sensors placed in the patient.

Clinical Measurements

A total of 31 sensors were implanted into the 18 patients and a total of 861 individual dose measurements were made. There were no unanticipated adverse events reported in association with the sensor placements and all devices performed successfully (one sensor did saturate prior of the end of therapy and reported a value of zero thereafter). Table 2 provides a summary for each sensor and each field configuration during treatment by tumor site. Both average discrepancy values (measured versus plan) and sensor standard deviation values are listed.

Several observations can be made based on the data in Table 2. Standard deviation values for less conformal fields are smaller. More conformal fields led to some standard deviation values in the 4–6% range, suggesting a random motion component. Such deviations might be addressed effectively by daily imaged-based localization. The normal tissue sensor in patient 16 showed extreme dose and standard deviation values. This sensor was outside, but close (~1 cm) to, the aperture edge and it was deduced that breathing motion lifted the sensor into the field for a significant fraction of the treatment time. The predicted dose of 21 cGy was routinely exceeded and the average error was over 450%. Thus this was a highly dynamic intrafractional phenomenon that is relatively easy to interpret.

A low standard deviation value does not necessarily correspond to a low average dose deviation value. As noted above, the standard deviation numbers are most useful in distinguishing random and systematic errors. If the standard deviation of the *in vivo* sensor readings exceeds the standard deviation of the sensor alone then random errors in setup or organ movement must be the cause. If the measured dose is routinely higher or lower than an amount accounted for by the absolute accuracy of the sensor (<1.8%; 1-sigma) then a systematic setup or plan error must be the cause. The data in Table 2 reveal several permutations: low random motion and low dose deviation (e.g., patient 05 tumor, 06 normal, 07 normal), low random motion and higher dose deviation (e.g., patient 01 tumor, 12 tumor), high random motion and low dose deviation (e.g., patient 12 boost), and high random motion and high dose deviation (e.g., patient 09 boost). Of course a high random motion and low dose deviation can result when the deviations average out over time. Patient 09 showed both a larger daily variation and a monotonic underdose, suggesting daily target mobility and a scalar error in the dose plan. For this patient, daily image-based localization alone would not necessarily rectify the dose discrepancy.

Figure 3 shows daily dose values from breast carcinoma patient 12. This patient was treated with tangential fields for 25 days and then was given an electron boost, *en face*. Only one sensor was placed in the tumor bed during a lumpectomy procedure. A retention “sock” was used to

secure the sensor in the lumpectomy cavity. Inhomogeneity correction was not used during the photon portion of therapy. The sensors were *not* specifically calibrated for electrons. Thus it is best to make qualitative conclusions only from the data collected during the boost. There is an apparent jump in the level of overdosing on about day 6 of therapy. The average error for the first 5 days is about 4.5% during this period and about 9.0% for the balance of the photon treatment. A port film taken on day 6 showed an apparent posterior shift of the beam aperture relative to the breast surface during simulation. (As can be seen on day 6 in figure 3, additional dose contributions from port films were added in an approximate manner to the predicted dose. The treatment plan did not include monitor units from the port films.) An offset of the sensor position in this direction in the isodose curve set is consistent with an increase in measured dose. This shift in the port film was realized retrospectively and the protocol did not allow for dose correction based on sensor data alone. It should be noted that the sensors used in this study do not show up well in megavoltage images and thus the sensors were not typically distinguished in port films. A version of the sensor has been tested that incorporates gold wire in the coil instead of copper wire and this change renders the coil section readily visible using EPID's and film-based portal imaging.

Figure 4 summarizes data from all of the patients (all dose readings) in the form of frequency of error (regardless of the sign of the error). The plot provides the percentage of dose measurements that equal or exceed an error of 5% and 8%. The 5% value was chosen as the maximum allowable planning error. It should be noted that in no patient did 5% or higher random variations about the target dose occur. That is, discrepancies of that magnitude were always of one sign or the other (over- or underdose) for a given field set. The 8% value was chosen as being indicative of magnitudes that are reported to lead to statistically less favorable outcomes (1), either lack of tumor control or excessive normal tissue morbidity. The patients are grouped by disease site. A few specific observations can be made. Patient 3 had a lesion that protruded beyond the chest wall and was very fluid-rich and the sensors were placed well within the field boundaries. Without the contributions from the inhomogeneity of alveolar tissue and without high dose gradients, the level of error recorded was lower. Prostate patients 10&11 did not receive the 6-field boost (where the greatest errors were recorded in the first two patients) and instead received I-125 brachytherapy. For breast patient 12 in figure 4, it has already been noted that a very suggestive alignment error was found that would explain the level of overdosing (note: only the photon data were included in figure 4). Going forward in testing the implantable dosimeter, additional planning CT's will be recorded and other checks will be made when dose errors indicate a potential problem. During the current study, again, dose data was not made available for possible plan corrections.

Figure 5 shows the *in vitro* data and data from all patients as histograms. The inner border indicates dose errors of 5% or greater and the outer border shows 8% or greater. The plot including all patients has a roughly Gaussian appearance, as one might expect. Of greater interest are the histograms of individual disease sites. Each of these classes of patient was treated at one institution (i.e., there is no mixing of data from multiple centers for a given disease site). The plot of the rectal patients looks, again, remarkably Gaussian given the small number of subjects and the variance of the curve is small, consistent with the values in Table 2. Yet there is a clear offset in the mean dose from the zero error point. The breast data show a positive offset and the prostate data show a negative offset (and a more asymmetric tail on the negative side). The lung data comprise a fairly centered distribution and the largest variance (reflecting the fact that the AP/PA plans tended to produce overdoses and the obliques tended to produce underdoses).

Discussion

This analysis of an implantable dosimeter system prompts two general topics of discussion: 1) *in vitro* versus *in vivo* considerations; 2) applications in institutional QA and IGRT and individual patient dose QA. The implanted dosimeters used in this pilot study produced a prodigious amount of data. To make this information useful in a clinical setting, an efficient means of presentation and analysis must be adopted for each application.

1. *In vitro* versus *in vivo* considerations

The *in vitro* data support the belief that under idealized conditions an error level of +/− 5% for dose delivery is achievable. If the subject is static in time, of uniform density, and rigid during setup and alignment then a level of accuracy consistent with machine commissioning will result. However, patients exhibit none of these attributes. The target within a patient may change over the course of therapy (6,7,8,9), a patient has significant, sometimes time-varying inhomogeneities (18,19,20), and a patient is not rigid nor can he often be immobilized adequately to guarantee consistent setup (28). If these non-idealities affect protocols in a more-or-less consistent way (e.g., by ignoring inhomogeneity factors) then the attributes of the histograms in figure 5 are not at all surprising. It may be the case that a given institution consistently deviates from the nominal dose plan. Thus the institution's clinical outcome experience may well be for these "distorted" dose protocols. If true, then immediately altering the dose mean, for instance, would not be prudent. What is created, however, is a situation wherein the comparison of outcomes from multiple independent institutions may be difficult because the effective delivered doses are not the same.

Many of the larger sensor deviations in the phantom measurements are correlated in sign suggesting small thermal drifts between the pre- and post-dose readings. The threshold voltage of the MOSFET's varies with temperature (24,26). An improved sensor, especially for in vitro work, would result if this thermal effect were reduced and if a sensor-based temperature monitor were included in the device (24). As noted earlier, the thermal effects will not be primary in patients since the sensors are placed at a minimum depth of 3 cm (25) and the two readings are taken within 30 minutes of each other. The implantable dosimeter can generate metrics of dose calculation accuracy in heterogeneous human tissue. Typically, heterogeneous phantom measurements are uncommon unless commissioning a TPS algorithm. The ability to run differing algorithms and grid resolutions in a TPS and optimize for accuracy versus *in vivo* dosimetric measurements would enable clinicians to optimize their treatment planning choices. Future clinical studies will aim to standardize the TPS dose algorithm (to Superposition, or Monte Carlo if available), modeling accurately the effects of heterogeneous patient tissue, with a high-resolution dose calculation spacing (3 mm or less in each axis).

The number of patients included in this study is small. There is no evidence that these results will prove to be typical in a larger study. However, it is interesting to note that 12 of 18 subjects in this study had 5% or larger dose deviations for at least 40% of all treatment sessions. It will be of particular interest to perform measurements in patients undergoing IMRT planning and treatment (this is underway) to see if more conformal plans present a different impression in a graph like figure 4. The only suggestion of what might be found is perhaps seen in the prostate patients for whom more frequent and large dose deviations were seen during the 6-field conformal boost treatment.

2. Applications in Institutional QA and IGRT and Individual Patient Dose QA

Institutional applications in QA and IGRT may be addressed by the histograms of patients partitioned by disease location. The conformance of these data to a Gaussian distribution is apparent, even with such small samplings (note that the subject number, "n" is listed in figure

5 and that most patients had 2 sensors placed). An institutional cause may be suggested for the apparent irregularities in the means.

Regular clinical use of the implantable dosimeters would provide important complementary data to IGRT localization. One can envision using the spread of dosimeter measurements versus TPS calculations at points to "measure" the success of new IGRT methods; i.e. the average dose deviation between measured and the ideal planned value should decrease with successful implantation of IGRT. Some common IGRT localization methods in use today include: 1) ultrasound localization of the prostate/bladder interface with overlaying reconstructions of the TPS contours; 2) MV EPID imaging of implanted gold seed fiducials or bony landmarks compared to TPS DRRs (digitally reconstructed radiographs); and 3) volumetric CT generated by TomoTherapy imaging/delivery machines (TomoTherapy, Inc.). Some quickly emerging IGRT localization methods include: 1) kV EPID imaging by on-board planar imaging devices on conventional C-arm linear accelerators; 2) CBCT (cone-beam CT) acquired by these on-board imaging devices; and 3) imageless localization via "beacons" (Calypso, Inc.) that can track location and movement of implanted probes. All of the aforementioned IGRT techniques track the location of points in the patient anatomy and allow for patient re-positioning prior to each treatment fraction. The implantable dosimeter would be an ideal fiducial marker for the kV and MV (with a gold coil in the dosimeter) EPIDs, CBCT, TomoTherapy CT, and even ultrasound imaging methods and could thus be complementary to the rapidly evolving IGRT technologies.

Another focus for the dosimeter system is obvious – effective delivery of dose at depth for individual patients. This may be addressed by examining the variation in expected and measured dose over the course of treatment, trying to prevent a trend of deviations from the expected value. Implantable dosimeters offer data over and above positional fiducial markers for IGRT, as the per-fraction measured dose generated by the dosimeter system allows for immediate risk management/QA procedures for the detection of medical events. While IGRT methods optimize the patient/target position prior to or during a fraction, they cannot detect dose discrepancies. A misadministration of dose could occur in several ways, such as improper dose rate calibration, improper or incomplete IMRT QA, or errors in MLC leaf sequences. All of these are undetectable by IGRT alone. Used together, IGRT and implantable dosimeters would allow clinicians to monitor target positioning and actual dose delivery.

Conceivably, the future may create a situation in which therapy plans are perfect in a time-dependent fashion, alignment and target tracking are perfect, and human errors are exceedingly rare. In such a future, the implanted dosimeter would perform closer in practice to a surface dosimeter, which is rarely expected to show a significant deviation from the plan. A more likely future is one in which margins are being reduced (9), plan complexity is being increased (4), localization tools may not always function as expected (6,7), and human error will remain. If radiotherapy is to remain true to its empirical roots then greater empiricism must be injected into an environment now being inundated by more complex simulations. It is of concern that many papers on dosimetry are actually nothing more than simulations of theoretical predictions. It is sobering to consider the number of assumptions and predictions that occur prior to patient treatment after the last truly empirical check executed is often in the form of a fluence map of the linear accelerator in a water phantom. The results of this pilot study suggest strongly that greater, not less, empiricism is needed to ensure consistent dose delivery at depth.

Finally, the implanted dosimeter enables future studies that seek to address the details of dose response. Imagine a case wherein a patient is overdosed for 1/2 of the treament period and underdosed for the remaining 1/2 (not unlike patient 01). Is this equivalent to no errors every day even though the cumulative effect balances out? Conventional dose-response studies were neither designed to answer this question nor could they even in principle without a means of

measuring dose at depth. It is well accepted that irreversible damage to DNA by radiation has a non-linear threshold. Certainly the underlying basis of accelerated dose protocols is that repair of sub-lethal damage in DNA can be influenced by time-integrated dose levels. It is also understood that late tissue effects, like the transformation of normal tissue due to sub-lethal incidental radiation exposure, can exhibit quite long times to progression. In both examples, knowing the exact time-dose profile would be helpful in categorizing outcomes. A recent study by Hanks et al. (29) has emphasized the importance of even small deviations in delivered dose. That study concluded that a difference of less than 6% in cumulative dose given to prostate patients resulted in a 65% change in disease-free status over time. To reiterate a point made in the Introduction, only by separating out the effects of inaccurate dose delivery can patient-dependent variations in response be understood.

Conclusion

This pilot study has demonstrated that the implantable dosimeter is an effective tool for quantifying dose at depth. Such a dosimeter could be used as a therametric device (measurements that guide the application of therapy) to guide, in conjunction with existing planning and delivery tools, the application of radiotherapy on an individual patient basis. Additionally, dose data from these sensors can be used collectively to evaluate adherence, on an institutional basis, to national dose protocols.

Acknowledgements

Work supported in part by NCI grant R21CA 97859. The authors gratefully acknowledge the efforts of Migdalia Acquino, Natasha Bolick, Dr. Greg Bortoff, Tammy Carrea, Theresa Dixon, Caroline Fraisse, Chris Rini, and Steve Widener.

References

1. Van Dyk J (ed.). The Modern Technology of Radiation Oncology. Madison, WI: Medical Physics Publishing; 1999.
2. Galvin JM, Ezzell G, Eisbrauch A, Yu C, Butler B, Xiao Y, Rosen I, Rosenman J, Sharpe M, Xing L, Xia P, Lomax T, Low DA, Palta J. Implementing IMRT in clinical practice: a joint document of the American Society for Therapeutic Radiology and Oncology and the American Association of Physicists in Medicine. Int J Radiat Oncol Biol Phys 2004;58:1616–34. [PubMed: 15050343]
3. Ezzell GA, Galvin JM, Low D, Palta JR, Rosen I, Sharpe MB, Xia P, Xiao Y, Xing L, Yu CX. Guidance document on delivery, treatment planning, and clinical implementation of IMRT: report of the IMRT Subcommittee of the AAPM Radiation Therapy Committee. Med Phys 2003;30:2089–115. [PubMed: 12945975]
4. Ramsey C, Dube S. It is necessary to validate each individual IMRT plan before delivery (Point/Counterpoint). Med Phys 2003;30:2271–2273. [PubMed: 14528945]
5. Lattanzi J, McNeely S, Hanlon A, Das I, Schultheiss TE, Hanks GE. Daily CT localization for correcting portal errors in the treatment of prostate cancer. Int J Radiat Oncol Biol Phys 1998;41:1079–1086. [PubMed: 9719118]
6. Langen KM, Pouliot J, Anezinos C, Aubin M, Gottschalk AR, Hsu IC, Lowther D, Liu YM, Shinohara K, Verhey LJ, Weinberg V, Roach M. Evaluation of ultrasound-based prostate localization for image-guided radiotherapy. Int J Radiat Oncol Biol Phys 2003;57:635–644. [PubMed: 14529767]
7. Van den Heuvel F, Powell T, Seppi E, Littrupp P, Khan M, Wang Y, Forman JD. Independent verification of ultrasound based image-guided radiation treatment, using electronic portal imaging and implanted gold markers. Med Phys 2003;30:2878–2887. [PubMed: 14655934]
8. Poggi MM, Gant DA, Sewchand W, Warlick WB. Marker seed migration in prostate localization. Int J Radiat Oncol Biol Phys 2003;56:1248–1251. [PubMed: 12873668]
9. Huang E, Dong L, Chandra A, Kuban DA, Rosen II, Evans A, Pollack A. Intrafraction prostate motion during IMRT for prostate cancer. Int J Radiat Oncol Biol Phys 2002;53:261–268. [PubMed: 12023128]

10. Paliwal BR, Brezovich IA. IMRT may be used to excess because of its higher reimbursement from Medicare (Point/Counterpoint). Med Phys 2004;31:1–3. [PubMed: 14761013]
11. Amols H, Williamson JF. The current NRC definitions of therapy misadministration are vague, do not reflect the norms of clinical practice, and should be rewritten (Point/Counterpoint). Med Phys 2004;31:691–694. [PubMed: 15124984]
12. Dutreix A. When and how can we improve precision in radiotherapy? Radiother Oncol 1984;2:275–292. [PubMed: 6522641]
13. Mijnheer BJ, Battermann JJ, Wambersie A. What degree of accuracy is required and can be achieved in photon and neutron therapy? Radiother Oncol 1987;8:237–252. [PubMed: 3107087]
14. Secomb TW, Hsu R, Dewhirst MW. Synergistic effects of hyperoxic gas breathing and reduced oxygen consumption on tumor oxygenation: a theoretical model. Int J Radiat Oncol Biol Phys 2004;59:572–578. [PubMed: 15145178]
15. Almond PR, Biggs PJ, Coursey BM, Hanson WF, Huq MS, Nath R, Rogers DW. AAPM's TG-51 protocol for clinical reference dosimetry of high-energy photon and electron beams. Med Phys 1999;26:1847–70. [PubMed: 10505874]
16. Fraass B, Doppke K, Hunt M, Kutcher G, Starkschall G, Stern R, Van Dyke J. AAPM Radiation Therapy Committee Task Group 53: Quality assurance for clinical radiotherapy treatment planning. Med Phys 1998;25:1773–1829. [PubMed: 9800687]
17. Ma C-M, Jiang SB, Pawlicki T, Chen Y, Li JS, Deng J, Boyer AL. A quality assurance phantom for IMRT dose verification. Phys Med Biol 2003;48:561–572. [PubMed: 12696795]
18. Orton CG, Mondalek PM, Spicka JT, Herron DS, Andres LI. Lung corrections in photon beam treatment planning: are we ready? Int J Radiat Oncol Biol Phys 1984;10:2191–2199. [PubMed: 6439697]
19. Frank SJ, Forster KM, Stevens CW, Cox JD, Komaki R, Liao Z, Tucker S, Wang X, Steadham RE, Brooks C, Starkschall G. Treatment planning for lung cancer: traditional homogeneous point-dose prescription compared with heterogeneity-corrected dose-volume prescription. Int J Radiat Oncol Biol Phys 2003;56:1308–1318. [PubMed: 12873675]
20. De Jaeger K, Hoogeman MS, Engelsman M, Seppenwoolde Y, Damen EM, Mijnheer BJ, Boersma LJ, Lebesque JV. Incorporating an improved dose-calculation algorithm in conformal radiotherapy of lung cancer: re-evaluation of dose in normal lung tissue. Radiother Oncol 2003;69:1–10. [PubMed: 14597351]
21. Essers M, Mijnheer BJ. In vivo dosimetry during external photon beam radiotherapy. Int J Radiat Oncol Biol Phys 1999;43:245–259. [PubMed: 10030247]
22. Svensson H. Quality assurance in radiation therapy: physical aspects. Int J Radiat Oncol Biol Phys 1984;10 (suppl 1):59–65. [PubMed: 6429102]
23. Tepper JE, Bortfeld T, Chen GTY (eds.). High-precision radiation therapy of moving targets. *Sem Radiat Oncol* 2004;14:1–100.
24. Scarantino CW, Ruslander DM, Rini CJ, Mann GG, Nagle HT, Black RD. An Implantable Radiation Dosimeter for use in External Beam Radiation Therapy. Med Phys 2004;31:2658–2671. [PubMed: 15487749]
25. Scarantino CW, Rini CJ, Aquino M, Carrea TB, Ornitz RD, Anscher MS, Black RD. The Initial Clinical Results of an *In Vivo* Dosimeter During External Beam Radiation Therapy. *Int J Radiat Oncol Biol Phys* (in press).
26. Beddar AS, Salehpour M, Briere TM, Hamidian H, Gillin MT. Preliminary evaluation of implantable MOSFET radiation dosimeters. Phys Med Biol 2005;50:141–149. [PubMed: 15715428]
27. Craig T, Brochu D, Van Dyk J. A quality assurance phantom for three-dimensional radiation treatment planning. Int J Radiat Oncol Biol Phys 1999;44:955–66. [PubMed: 10386655]
28. Bentel GC, Munley MT, Marks LB, Anscher MS. The effect of pressure from the table top and patient position on pelvic organ location in patients with prostate cancer. Int J Radiat Oncol Biol Phys 2000;47:247–253. [PubMed: 10758331]
29. Hanks GE, Hanlon AL, Epstein B, Horwitz EM. Dose response in prostate cancer with 8–12 years' follow-up. Int J Radiat Oncol Biol Phys 2002;54:427–435. [PubMed: 12243818]

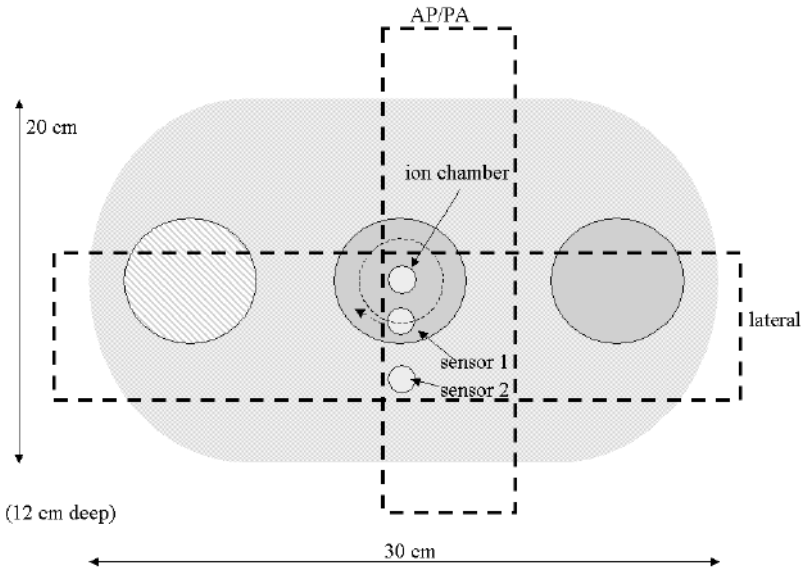

Figure 1.
Acrylic phantom indicating the locations of the 2 implantable sensors and the ion chamber.

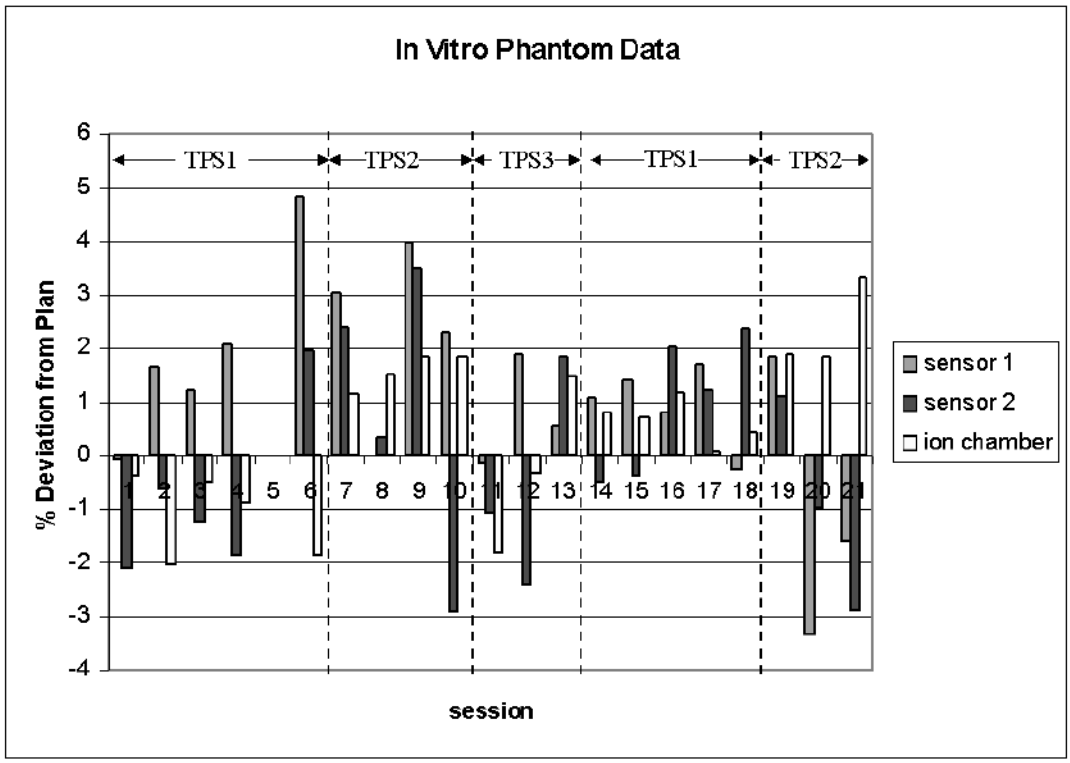

Figure 2.
Phantom data using multiple TPS plans.

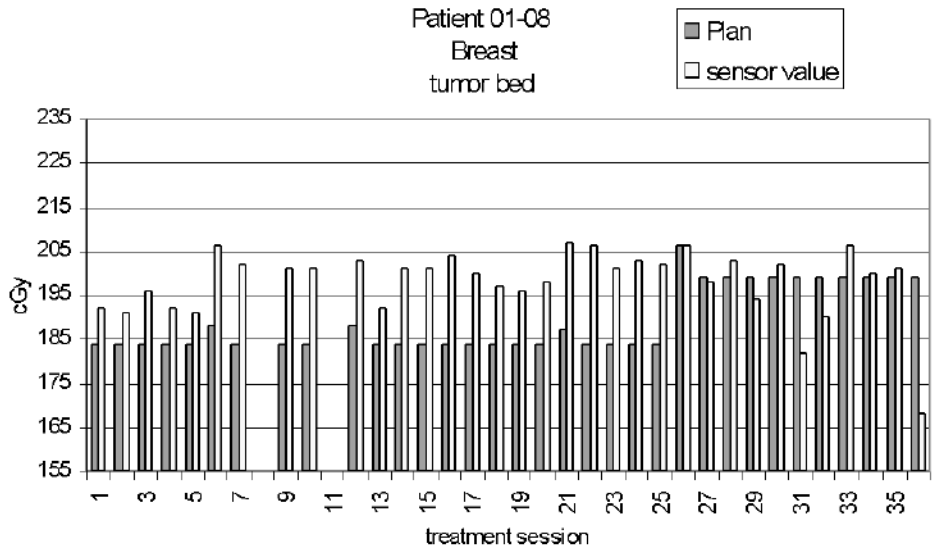

Figure 3.
Patient 12 daily dose readings. An electron boost started on session 26. (Readings were missed on days 8 & 11.) Port films were taken on days 6, 12, 21, and 26.

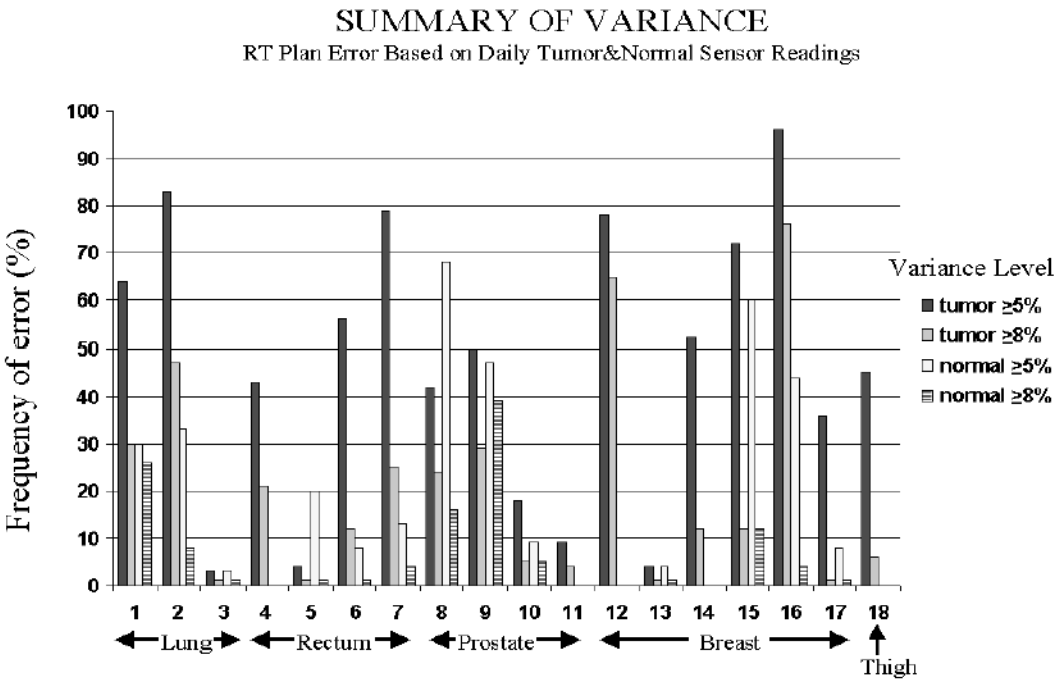

Figure 4.
Variance from predicted dose values for patients in this study.

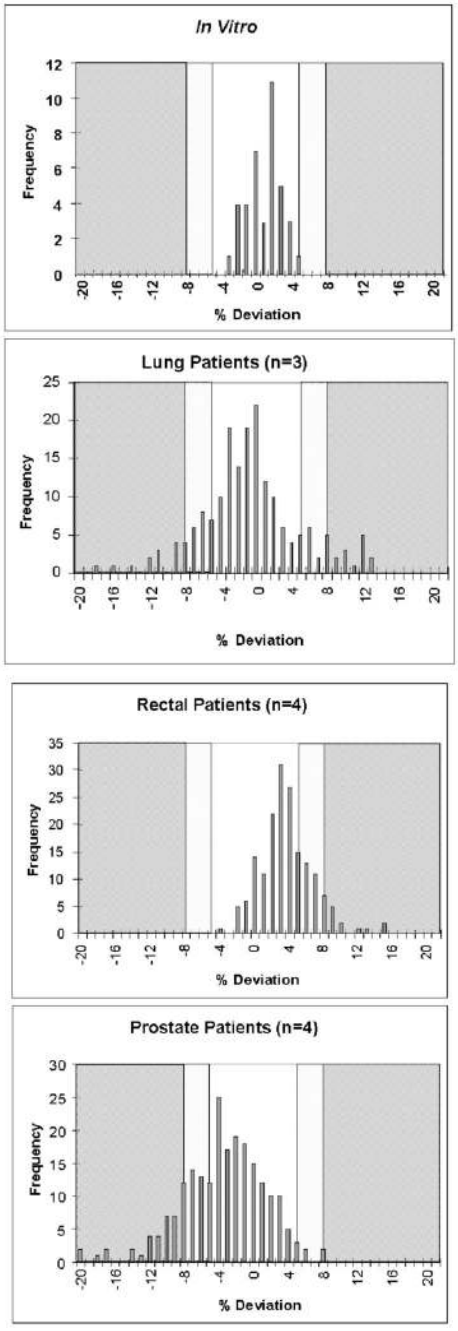

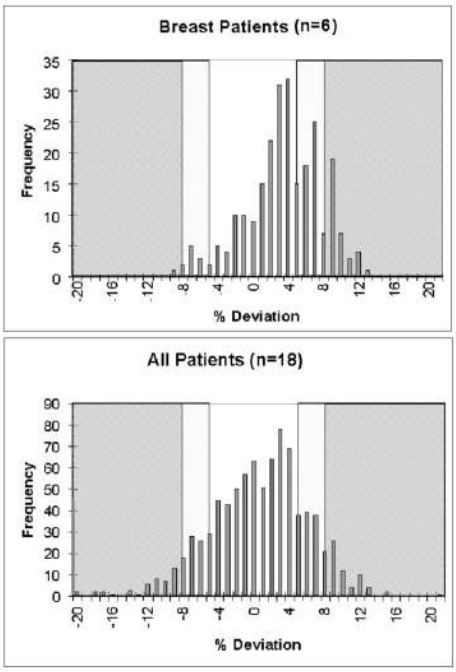

Figure 5.
Histograms of patient data by disease area and of results from the *in vitro* study.

Table 1

Patient planning details

Patients 1–7 and 12–18 were planned using the Pinnacle (6.2b) treatment planning system. The planning grid was 0.4 cm in each dimension. An adaptive convolution algorithm was used for all photon plans and Pinnacle's Electron 3D algorithm was used for electron boost plans. Patients 8–11 were planned using the PLUNC treatment planning system, which uses a modified Clarkson method. The planning grid dimensions were 0.5 cm in each dimension. PLUNC performs scatter correction with a differential scatter-air ratio algorithm and corrects for tissue inhomogeneities using the Batho power law model (25). All dose values were calculated as point doses by identifying the MOSFET in the planning CT data set and using a cursor to identify a point dose in the isodose map. All planning CT's used 3 mm slice thickness. The therapy machine type and inhomogeneity correction usage are listed.

AP = anterior-to-posterior ; LAO = lateral anterior oblique; Lats = bi-lateral; LLT = left lateral tangential; LMT = left medial tangential; LPO = lateral posterior oblique; PA = posterior-to-anterior; RLT = right lateral tangential; RMT = right medial tangential; RPO = right posterior oblique; W indicates the use of wedge

A: Lung patient #	**field set 1**	**field set 2**	**field set 3 (boost)**
01	(day 1–20) AP: 6MV PA: 6MV Clinac 1800 homogeneous	(day 21–28) LAO: 6MV RPO: 6MV Primus-M heterogeneous	(day 29–34) LAO: 6MV,W RPO: 6MV,W Primus-M heterogeneous
02	(day 1–21) AP: 6MV,W PA: 6MV Primus-M homogeneous	(day 22–31) LAO: 6MV RPO: 6MV Primus-M heterogeneous	(day 32–36) LAO: 6MV RPO: 6MV Primus-M heterogeneous
03	(day 1–22) AP: 6MV,W PA: 18MV,W LPO: 6MV Clinac 1800 homogeneous	(day 23–29) RAO: 6MV LPO: 6MV Clinac 1800 heterogeneous	none

B: Rectal patient #	**field set 1**	**field set 2 (boost)**
04	(day 1–25) AP/PA: 18MV Lats: 18MV Clinac 2100 homogeneous	(day 26–28) PA: 6MV Lats: 18 MV,W Clinac 2100 homogeneous
05	(day 1–25) AP/PA: 18MV Lats: 18MV Clinac 2100 homogeneous	none
06	(day 1–25) AP/PA: 18MV Lats: 18MV Clinac1800 homogeneous	none
07	(day 1–25) AP/PA: 18MV Lats: 18MV Clinac 1800 homogeneous	none

C: Prostate patient #	**field set 1**	**field set 2 (boost)**
08	(day 1–23) AP/PA: 6MV Lats: 6MV Mevatron MXE-2 heterogeneous	(day 24–39) 6-field: 6MV Mevatron MXE-2 heterogeneous
09	(day 1–23)	(day 24–39)

C: Prostate patient #	field set 1	field set 2 (boost)
	AP/PA: 6MV Lats: 6MV Mevatron MXE-2 heterogeneous	6-field: 6MV Mevatron MXE-2 heterogeneous
10	(day 1–23) AP/PA: 6MV Lats: 6MV Mevatron MXE-2 heterogeneous	I–125 seeds (no device reading)
11	(day 1–23) AP/PA: 6MV Lats: 6MV Mevatron MXE-2 heterogeneous	I–125 seeds (no device reading)

D: Breast patient #	field set 1	electron boost*(en face)*
12	(day 1–25) LMT:6MV,W LLT:6MV,W LLT:6MV Clinac 1800 homogeneous	(day 26–36) 12 MeV Clinac 1800 homogeneous
13	(day 1–25) LMT:6MV,W LMT:18MV,W LMT:6MV LLT:6MV,W LLT:18MV,W LLT:6MV Clinac 1800 homogeneous	(day 26–36) 16MeV Clinac 1800 homogeneous
14	(day 1–25) AP: 6MV RMT:6mV,W RLT:6MV,W RLT:6MV Clinac 1800 homogeneous	(day 26–36) 12MeV Clinac 1800 homogeneous
15	(day 1–25) AP:6MV RMT:6MV,W RMT:18MV,W RLT:6MV,W RLT:18MV,W RLT:18MV Clinac 1800 homogeneous	(day 26–36) 12MeV Clinac 1800 homogeneous
16	(day 1–25) RMT:6MV,W RLT:6MV,W RLT:6MV Primus-M homogeneous	(day 26–36) 16MeV Clinac 1800 heterogeneous
17	(day 1–25) LMT:6MV,W LLT:6MV,W LLT:6 MV Primus-M homogeneous	(day 26–36) 12MeV Clinac 1800 homogeneous

Table 2

Patient dose measurement details

The average deviation of each sensor with respect to plan is listed (expressed as a percentage) as well as the planned dose (at the sensor position). Overdoses (+) and underdoses (−) are indicated by sign. Standard deviations of each sensor are also listed (expressed as a percentage). The normalized (to planned dose) average measured dose was used to normalize the standard deviation values. The patient data consists of: 3 lung patients (**A**), 4 rectal patients (**B**), 4 prostate patients (**C**), 6 breast patients (**D**), and 1 patient (**E**) with a sarcoma in an extremity (thigh). Monitor units contributed by port films were added to the target dose values in an approximate fashion for comparison with sensor values.

A: Lung patient #/sensor location	**% deviation field set 1**	**% deviation field set 2**	**% deviation boost**	**% std. dev. field set 1**	**% std. dev. field set 2**	**% std. dev. boost**
01 tumor	5.2/0.5%* plan:191/200* cGy	−7.5% plan: 198 cGy	−3.5% plan: 191 cGy	2.94%	2.40%	3.67%
01 norm.tiss.	−1.4/−0.4%* plan:198/196* cGy	−12.1% plan: 198 cGy	out of field	2.43%	4.77%	out of field
02 tumor	8.4/1.3%* plan:200/214* cGy	−4.6% plan: 219 cGy	sensor out of range plan: 213 cGy	2.81%	2.79%	sensor out of range
02 norm. tiss.	−0.2/2.8%* plan:204/198* cGy	−5.9% plan: 207 cGy	−5.8% plan: 201 cGy	1.88%	2.72%	1.96%
03 tumor	−0.5% plan: 189 cGy	−2.4% plan: 184 cGy		2.29%	1.07%	
03 tumor	−1.0% plan: 190 cGy	−2.2% plan: 186 cGy		2.14%	0.83%	

B: Rectal patient #/sensor location	**% deviation field set 1**	**% deviation boost**	**% std. dev. field set 1**	**% std. dev. boost field**
04 tumor	3.4% plan: 194 cGy	11.9% plan: 166 cGy	3.16%	4.28%
05 tumor	1.7% plan: 186 cGy		1.82%	
05 norm. tiss.	3.1% plan: 186 cGy		1.86%	
06 tumor	4.8% plan: 186 cGy		2.27%	
06 norm. tiss.	2.0% plan: 186 cGy		2.19%	
07 tumor	7.7% plan: 188 cGy		2.19%	
07 norm. tiss.	3.3% plan: 186 cGy		1.89%	

C: Prostate patient #/sensor location	**% deviation field set 1**	**% deviation boost**	**% std. dev. field set 1**	**% std. dev. boost**
08 tumor	−1.2% (day 1–14) −3.8% (day 15–23) plan: 207 cGy	−7.2% (day 24–39) plan: 204 cGy	1.65% (day1–14) 1.45% (day15–23)	4.30%
08 tumor	−4.9% (day 1–14) −6.3% (day 15–23) plan: 207 cGy	−5.5% (day 24–39) plan: 201 cGy	1.69% (day 1–14) 1.29% (day 15–23)	4.39%
09 tumor	−1.2% (day 1–14) −4.4% (day 15–23) plan: 208 cGy	−8.1% (day 24–39) plan: 209 cGy	1.25% (day 1–14) 2.30% (day 15–23)	4.49%
09 norm. tiss.	−0.4% (day 1–14)	−11.5%	1.46% (day 1–14)	6.35%

C: Prostate patient #/sensor location	% deviation field set 1	% deviation boost	% std. dev. field set 1	% std. dev. boost
	−5.3% (day 15–23) plan: 205 cGy	(day 24–39) plan: 207 cGy	2.29% (day 15–23)	
10 tumor	2.1% (day 1–23) plan: 198 cGy	I-125 seeds (no device reading)	2.32%	
10 norm. tiss.	1.8% (day 1–23) plan: 198 cGy	I-125 seeds (no device reading)	2.32%	
11 tumor	−3.5% (day 1–23) plan: 208 cGy	I-125 seeds (no device reading)	1.46%	

D: Breast patient #/sensor location	% deviation field set 1	% deviation electron boost	% std. dev. field set 1	% std. dev. electron boost
12 tumor bed	8.0% plan: 184 cGy	−2.1% plan: 199 cGy	2.24%	5.67%
13 tumor bed	0.2% plan: 188 cGy	8.1% plan: 156 cGy	1.91%	3.33%
13 norm. tiss.	2.3% plan: 193 cGy	2.4% plan: 195 cGy	1.43%	2.02%
14 tumor bed	−4.7% plan: 187 cGy	−9.3% plan: 178 cGy	2.91%	3.29%
15 tumor bed	6.1% plan: 187 cGy	0.9% plan: 200 cGy	1.89%	4.30%
15 norm. tiss.	5.2% plan: 187 cGy	out of field	2.01%	out of field
16 tumor bed	8.4% plan: 186 cGy	−2.7% plan: 218 cGy	1.87%	3.67%
16 norm. tiss.	3.9% plan: 191 cGy	453% plan: 21 cGy (nearly out of field)	2.47%	41.9%
17 tumor bed	3.6% plan: 185 cGy	−10.0% plan: 200 cGy	2.39%	2.44%
17 norm. tiss.	2.4% plan: 186 cGy	−7.6% plan: 161 cGy	2.04%	5.54%

* without/with inhomogeneity correction (uncorrected plan used for treatment)